Precipitation of Spherical Magnesium(II) Cresolate Particles

ARTICLE *in* CHEMISTRY OF MATERIALS · DECEMBER 2002

Impact Factor: 8.35 · DOI: 10.1021/cm020802o

Precipitation of Spherical Magnesium(II) Cresolate Particles

Timothy J. Boyle,* Eric N. Coker, Cecilia A. Zechmann, James A. Voigt, Mark A. Rodriguez, and Richard A. Kemp

Sandia National Laboratories, Advanced Materials Laboratory, 1001 University Boulevard SE, Albuquerque, New Mexico 87106

Michael Zum Mallen

Union Carbide Corporation, A Subsidiary of The Dow Chemical Company, 3333 Highway 6 South, Houston, Texas 77082

Received July 30, 2002. Revised Manuscript Received October 14, 2002

Magnesium bis-*o*-cresol (or *o*-methylphenoxide), $[Mg(oMP)_2]_n$ (**1**), was prepared through a variety of synthetic routes that involved the stoichiometric reaction of *o*-methylphenol (H-oMP), with $Mg(Bu)_2$, $Mg\{N(Si(CH_3)_3)_2\}_2(THF)_2$, or the bulk metal ($Mg^0$). In all cases the low-temperature product was found to be soluble, while precipitation occurred at higher temperatures. The precipitate could only be redissolved by the addition of pyridine or a similarly strongly coordinating Lewis base. The pyridine and NH_3 adducts of **1** were isolated as monomeric species, whereas the THF adduct proved to be the dimeric $[Mg(\mu\text{-oMP})(oMP)(THF)_2]_2$, **2**. For a limited set of conditions, sufficient control over the precipitation kinetics of the reaction between $Mg(Bu)_2$ and H-oMP was realized to yield spherical morphologies. The window of spherulitic growth was small and could only be partially controlled by varying reaction conditions during the precipitation. Use of seed particles to control nucleation events during precipitation was found to lead to increased monodispersity of spherical $[Mg(oMP)_2]_n$ precipitate powders.

Introduction

Heterogeneous Ziegler−Natta (Z−N) catalysts are used worldwide to generate polypropylene (PP) resins.[1] Typically, Z−N catalysts consist of a transition metal salt mixed with a main group metal alkyl. Some of the first components used to produce high selectivity Z−N catalysts were titanium(IV) chloride and aluminum alkyls. This mixture is believed to generate, in situ, a transition metal that possesses a metal−carbon bond (the active site) that can be repeatedly inserted into, to form the growing polymer chain. The degree of stereoregularity among PP polymers can vary considerably from catalyst to catalyst and is mainly associated with differences in the preparation of the heterogeneous catalysts.[1,2]

As generations of heterogeneous PP catalysts have evolved, there has been a greater emphasis on preparing catalysts that possess not only high activity and selectivity but also a high degree of morphological control. This interest stems from a need to improve reactor operability by lowering the amount of "fines", thereby greatly simplifying the handling of the polymer granules during standard operations.[3] The term "fines" is defined as polymer particulates that are significantly smaller than those of optimal size. In an attempt to anchor and disperse the transition metal to generate more uniform and active heterogeneous catalysts, various supports have been investigated wherein magnesium chloride ($MgCl_2$) has found the greatest utility. A nonmorphology-controlled version of the $MgCl_2$ support can be generated from $Mg(OEt)_2$ through a series of metathesis reactions and washes with $TiCl_4$.[1−3]

We have recently synthesized and characterized a series of magnesium aryloxides $[Mg(OAr)_2]_n$ as mono-, di-, and trinuclear species dependent on the conditions of synthesis.[4] Typically, these compounds demonstrate increased solubility in comparison to aliphatic hydrocarbon ligated $Mg(OR)_2$. This characteristic allows these compounds to be precipitated in a controlled manner and may allow for the production of particles with controlled morphologies which are also monodisperse in distribution. While several $Mg(OAr)_2$ precursors have been investigated, the *o*-cresol [*o*-methylphenol (OC_6H_4-2-(CH_3) or H-oMP] ligated species has been found to produce spherical particles when precipitated under specific experimental conditions. This report discusses the synthesis, structure, and morphology of "$Mg(oMP)_2$" under a variety of conditions.

* To whom correspondence should be addressed. Phone: (505)272-7625. Fax: (505)272-7336. E-mail: tjboyle@Sandia.gov.

(1) Moore, E. P., Jr. *Polypropylene Handbook*; Hanser/Gardner Publications: Cincinnati, OH, 1996.

(2) Moore, E. P., Jr. *The Rebirth of Polypropylene: Supported Catalysts. How the People of the Montedison Laboratories Revolutionized the PP Industry*; Hanser Publishers: Munich, Germany, 1998.

(3) Internal reports limited to Union Carbide Corporation.

(4) Zechmann, C. A.; Boyle, T. J.; Rodriguez, M. A.; Kemp, R. A. *Polyhedron* **2000**, *19*, 2557.

10.1021/cm020802o CCC: $25.00
Published on Web 12/13/2002

Experimental Section

All compounds were handled under an inert atmosphere using standard glovebox or Schlenk techniques. All solvents were freshly distilled from the appropriate drying agent and immediately stored over molecular sieves.[5] The following chemicals were used as received (Aldrich): magnesium metal (Mg^0), 1.0 M di-*n*-butylmagnesium in heptane ($Mg(Bu)_2$, sure seal bottle), *o*-cresol (H-oMP, 99+%), and hexamethyldisilazane (99.9%). $Mg\{N(Si(CH_3)_3)_2\}_2(THF)_2$ was prepared according to literature reports.[6]

^1H and ^{13}C NMR solution spectral data were collected on a Bruker 400-MHz spectrometer. All ^1H spectra were referenced against the residual proton impurity in the appropriate dried, deuterated solvent. FT-IR data were obtained on a Bruker Vector 22 spectrometer using KBr pressed pellets under a N_2 purge. Elemental analyses were performed on a Perkin-Elmer 2400 CHN−S/O elemental analyzer. Scanning electron microscopy (SEM) was carried out on an Amray 1830 instrument. Samples were prepared by placing a small amount of dried sample on a piece of carbon tape attached to an scanning electron microscope stub. The excess sample was tapped off and the stubs were transferred to a sputter chamber. After a gold or platinum layer was applied, the sample was transferred to the scanning electron microscope for analysis. Aside from the brief transfer in to and out of the sputter chamber, the samples were handled under an inert or vacuum atmosphere.

$[Mg(oMP)_2]_n$, 1. *Method 1.* H-oMP (16.5 g, 153 mmol) was dissolved in THF (40.0−50.0 mL) and slowly transferred (via cannula) to a stirred 0 °C solution containing $Mg(Bu)_2$ (76.0 mL, 76.0 mmol) diluted with THF (76.0 mL). The transfer was complete after 1 h. The resulting clear colorless solution was allowed to warm slowly to room temperature with stirring. After 12 h, a large amount of white precipitate had formed. The mixture was heated to reflux temperature for 4 h and cooled to room temperature, and the solvent was removed in vacuo to yield a fine white powder. Yield: 18.0 g (99%). FT-IR (KBr pellet): 3065(w), 3016(w), 2966(w), 2943(m), 2924(m), 2856(w), 1900(w), 1784(w) 1600(s), 1579(m), 1492(s), 1461(m), 1438(m), 1293(m), 1251(s), 1189(m), 1155(w), 1115(s), 1049(m), 980(w), 933(w), 861(s), 758(s), 717(m), 611(s), 588(m), 552(w), 518(m), 492(w). Anal. Calcd (found) for $C_{14}H_{14}MgO_2$: 70.48 (70.50) %C; 5.92 (6.14) %H.

Method 2. A THF solution containing H-oMP (5.35 g, 49.5 mmol) was slowly transferred to a 0 °C stirred solution containing $Mg\{N(Si(CH_3)_3)_2\}_2(THF)_2$ (9.41 g, 22.6 mmol) dissolved in a toluene/THF mixture (30.0/40.0 mL). The resulting clear colorless solution was stirred at 0 °C for 20 min and then placed in a room-temperature water bath and stirred for 24 h, after which time a large amount of precipitate had formed. The reaction was then heated at reflux temperatures for 3.5 h and cooled to room temperature and the solvent was removed in vacuo. The resultant off-white solid was washed with ≈100 mL of THF and dried under vacuum. Yield: 4.94 g (92%). FT-IR (KBr pellet): 3064(w), 3016(w), 2966(w), 2942(m), 2856(w), 1900(w), 1783(w) 1694(w), 1599(s), 1579(m), 1491(s), 1461(m), 1442(m), 1293(m), 1251(s), 1189(m), 1155(w), 1048(m), 980(w), 932(w), 861(s), 757(s), 717(m), 610(s), 588(m), 553(w), 519(m), 493(w), 431(m), 411(w). Anal. Calcd (found) for $C_{14}H_{14}MgO_2$: 70.48 (68.82) %C; 5.92 (5.99) %H.

Method 3. Under an argon flow, Mg^0 metal (0.801 g, 33.0 mmol), H-oMP (8.10 g, 74.9 mmol), and THF (100 mL) were placed in a three-neck round-bottom flask and cooled in an ice bath. Anhydrous NH_3 was bubbled through the mixture to initiate the reaction. When gas evolution became vigorous, the NH_3 stream was turned off and the reaction allowed to proceed at 0 °C. NH_3 was introduced intermittently to reinitiate or accelerate the reaction until the metal had been entirely consumed. The total reaction time was ≈16 h. The reaction was heated to reflux temperatures for ≈4 h, after which a white precipitate had formed. The remaining solution was decanted and the solid dried under vacuum, yielding a white powder. Yield: 6.0 g (76%). FT-IR (KBr pellet): 3359(m), 3272(w), 3063(w), 3016(m), 2969(w), 2943(w), 2923(w), 2858(w), 1598(s), 1579(m), 1488(s), 1460(m), 1444(m), 1377(w), 1293(m), 1253(s), 1217 (m), 1189(m), 1154(w), 1114(s), 1044(m), 979(w), 930(w), 861(s), 756(s), 717(m), 610(s), 580(m), 554(m), 518(m), 444(m), 429(m). Anal. Calcd (found) for $C_{28}H_{31}Mg_2NO_4$: 68.06 (67.99) %C; 6.32 (6.26) %H; 2.83 (2.40) %N.

$[Mg(\mu\text{-oMP})(oMP)(THF)_2]_2$, 2. This compound was prepared using Method 1 as described above with the following variations. After the two solutions were combined to obtain the final clear colorless 0 °C solution, the solution was concentrated under vacuum and placed in a −20 °C freezer. After several hours, a large number of X-ray quality crystals had formed. ^1H NMR (400.1 MHz, THF-d_8): δ 6.78 (1H, s, OC_6H_4-2-CH_3), 6.81 (2H, s, OC_6H_4-2-CH_3), 6.36 (1H, s, OC_6H_4-2-CH_3), 2.21 (3H, s, OC_6H_4-2-CH_3). $^{13}C\{^1H\}$ NMR (100.1 MHz, THF-d_8): δ 163.7 (OC_6H_4-2-CH_3), 130.7 (OC_6H_4-2-CH_3), 128.0 (OC_6H_4-2-CH_3), 126.9 (OC_6H_4-2-CH_3), 120.8 (OC_6H_4-2-CH_3), 115.4 (OC_6H_4-2-CH_3), 18.5 (OC_6H_4-2-CH_3). FT-IR (KBr pellet): 3063(w), 3015(m), 2973(m), 2929(m), 2879(w), 1598(s), 1578(m), 1489(s), 1460(m), 1448(m), 1377(w), 1327(w), 1293(m), 1252(s), 1189,(w) 1154(w), 1114(s), 1069(w), 1044(m), 1029(m), 980(w), 926(w), 861(s), 757(s), 717(m), 609(s), 578(m), 554(m), 517(m), 477(m), 442(m), 432(m). Anal. Calcd (found) for $C_{28}H_{28}Mg_2O_4$: 69.03 (66.70) %C; 7.90 (7.69) %H.

Structure Determination.[7] A suitable crystal of **2** was mounted on a glass fiber from a pool of Fluorolube HO-125 and then immediately placed under a liquid N_2 stream boil-off on a Bruker AXS diffractometer. The radiation used was graphite monochromatized Mo Kα radiation ($\lambda = 0.71073$ Å). Structural solutions were carried out using SMART Version 5.054, SAINT+ 5.02, SHELXTL 5.1 software, and XSHELL 3.0 software.[7] No absorption correction was performed. The structure was solved using direct methods, which yielded positions for the heavy atoms. Subsequent Fourier synthesis gave the remaining non-hydrogen atom positions. A severely disordered THF molecule was found in the lattice with four solvent molecules in the unit cell. Attempts to model the lattice THF were unsuccessful and the program PLATON/SQUEEZE was used to remove the THF solvent density. Hydrogen atoms were fixed in positions of ideal geometry and refined within the XSHELL software.[7] These idealized hydrogen atoms had their isotropic temperature factors fixed at 1.2 or 1.5 times the equivalent isotropic temperature factor (U) of the C atoms to which they were bonded. The final refinements include anisotropic thermal parameters on all non-hydrogen atoms. Data collection parameters are given in Table 1.

Results and Discussion

Synthesis. Three different magnesium reagents were utilized to prepare $[Mg(oMP)_2]_n$, **1**. In each reaction, a slight excess of *o*-cresol (H-oMP) was added to a solution or mixture containing the metal species (eqs 1−3). For eqs 1 and 3 a gaseous byproduct was formed, while in eq 2 the byproduct was a liquid that was then removed under vacuum. For the reaction mixtures of eq 1 or eq

$$Mg(Bu)_2 + 2H\text{-oMP} \rightarrow [Mg(oMP)_2]_n + 2H\text{-Bu} \quad (1)$$

$$Mg\{N(Si(CH_3)_3)_2\}_2(THF)_2 + 2H\text{-oMP} \rightarrow [Mg(oMP)_2]_n + 2HN(Si(CH_3)_3)_2 \quad (2)$$

$$Mg^0 + 2H\text{-oMP} \xrightarrow{NH_3(l)} [Mg(oMP)_2]_n + 2H_2 \quad (3)$$

(5) Perrin, D. D.; Armarego, W. L. F. *Purification of Laboratory Chemicals*, 3rd ed.; Pergamon Press: New York, 1988.

(6) Bradley, D. C.; Hursthouse, M. B.; Ibrahim, A. A.; Malik, K. M. A.; Motevalli, M.; Moseler, R.; Powell, H.; Runnacles, J. D.; Sullivan, A. C. *Polyhedron* **1990**, *9*, 2959.

(7) The listed versions of SAINT, SMART, XSHELL, and SADABS Software from Bruker Analytical X-ray Systems Inc., 6300 Enterprise Lane, Madison, WI 53719, were used in analysis.

Table 1. Data Collection Parameters for 2

compound	**2**
chemical formula	$C_{48}H_{68}Mg_2O_9$
formula weight	418.285
temperature (K)	168
space group	monoclinic
crystal system	*C*2/*c*
a (Å)	16.808(3)
b (Å)	16.080(3)
c (Å)	17.714(3)
β (°)	103.243(3)
V (Å^3)	4660.2(13)
Z	4
D_{calcd} (Mg/m^3)	1.194
μ (mm^{-1})	0.104
R1[a] (%)	10.26
wR2[b](%)	28.67
[$I > 2\sigma(I)$]	
R1[a] (%, all data)	23.47
wR2[b] (%, all data)	35.35

[a] $R1 = {}^{\sigma}||F_o| - |F_c||/\sigma|F_o|$. [b] $wR2 = [\Sigma[w(F_o^2 - F_c^2)^2]/\Sigma[w(F_o^2)^2]]^{1/2}$.

2, a precipitate formed upon warming the reaction to room temperature, which is thought to be a $[Mg(oMP)_2]_n$ (**1**) polymer. The solid product was subsequently isolated by vacuum distillation of the solvent. In contrast, when the ammonia route (eq 3) was used, no precipitate formed upon warming to room temperature; however, precipitation of this reaction could be induced by warming the reaction to reflux temperatures.

If the reaction in eq 1 was performed at room temperature, precipitation rapidly occurred. Single crystals were grown from "cold" reaction mixtures and single-crystal X-ray diffraction experiments showed the product to be the THF adduct, $[Mg(\mu\text{-oMP})(oMP)(THF)_2]_2$ (**2**). Compound **2** is stable in neat THF but unstable in noncoordinating solvents, immediately forming a precipitate upon introduction of toluene or hexanes. Compound **2** is also unstable in room-temperature THF/heptane mixtures; however, no change is observed for solutions when the reaction mixture is held at <8 °C for >12 h (THF/heptane = 1.5/1). Scheme 1 depicts a proposed pathway by which the soluble species, A, is converted into an insoluble oligomer, B. The scheme depicts the growth of **1** by means of solvent loss (step i), which opens a coordination site at a metal center, followed by coupling through terminal oMP groups (step ii). These types of solution interactions must be taken into account when attempting to understand parameters that affect nucleation, growth, and morphology of the particles isolated for this system.

Characterization. On the basis of FT-IR data, the bulk samples obtained from these disparate methods are nearly identical. Of note in the spectrum of the NH_3 route (eq 3) product are stretches in the 3400−3200-cm^{-1} range, which can be attributed to N−H stretching vibrations and suggests the presence of metal-bound NH_3.[8] Elemental analysis also revealed the retention of NH_3, quantified as $1NH_3/2Mg$. The elemental analyses of products from the alkyl and amide routes detected no nitrogen. In all cases, the product powder could be redissolved in the presence of strong donor solvents (e.g., pyridine), but displayed limited or no solubility in THF, aromatic, and aliphatic solvents.

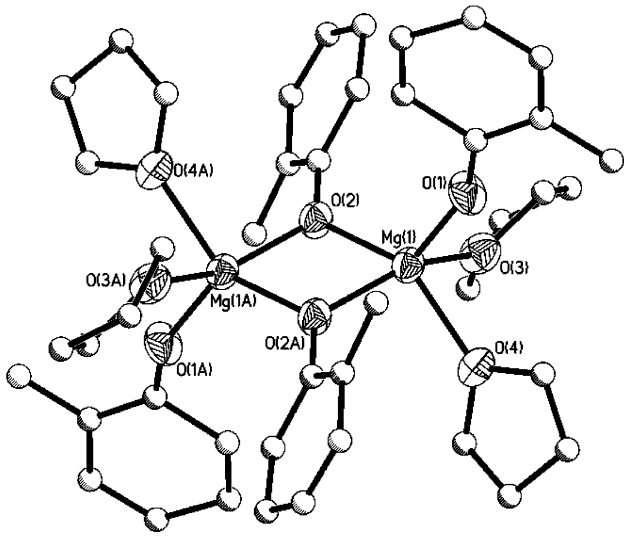

Figure 1. Thermal ellipsoid plot of $[Mg(\mu\text{-oMP})(oMP)(THF)_2]_2$ (**2**).

X-ray Structures. Shown in Figure 1 is the thermal ellipsoid plot of $[Mg(\mu\text{-oMP})(oMP)(THF)_2]_2$, **2**. Table 1 contains a listing of the crystallographic data. The molecule was found to be dinuclear with each five-coordinate Mg adopting a trigonal bipyramidal geometry through the binding of two bridging and one terminal oMP ligand. The two final coordination sites on each metal center are occupied by THF solvent molecules. This structure is similar to previously reported dinuclear Mg compounds, $[Mg(\mu\text{-OR})(OR)(Solv)]_2$ (OR = $OSi(C_6H_5)_3$, $OC(CH_3)(C_6H_5)_2$; Solv = THF, py).[4] In these complexes, the large steric demands of the ligands limits the number of coordinated solvent molecules wherein each four-coordinate Mg adopts a pseudo-tetrahedral arrangement. Due to the quality of the final structure of **2**, the metrical data cannot be discussed in depth; however, as is generally observed, the shortest M−O bond distances are the terminal oMP groups while the bridging Mg−O bonds are slightly longer and the Mg−Solv distances the longest.[4 9−13]

Solution NMR of **2**. If the solid-state structure of **2** remains intact upon dissolution, two ligand environments should be present. We obtained variable-temperature ^{1}H NMR spectra of **2** in THF-d_8 for a concentrated and a dilute sample. For the dilute sample, the ^{1}H NMR spectrum revealed a single oMP environment at room temperature while the concentrated sample showed an additional minor set of resonances in both the phenyl and methyl regions. From −20 to −60 °C, one set of resonances was observed in the concentrated sample corresponding to the major species observed at room temperature. The ^{13}C NMR spectra of these samples gave analogous results. The multiple resonances observed by the variations in both concentration and temperature is most likely explained by the presence of multiple species in solution, such as an equilibrium

(8) Butcher, R. J.; Clark, D. L.; Grumbine, S. K.; Vincent-Hollis, R. L.; Scott, B. L.; Watkin, J. G. *Inorg. Chem.* **1995**, *34*, 5468.

(9) Bradley, D. C.; Mehrotra, R. C.; Gaur, D. P. *Metal Alkoxides*; Academic Press: New York, 1978.

(10) Bradley, D. C. *Chem. Rev.* **1989**, *89*, 1317.

(11) Chandler, C. D.; Roger, C.; Hampden-Smith, M. J. *Chem. Rev.* **1993**, *93*, 1205.

(12) Hubert-Pfalzgraf, L. G. *New. J. Chem.* **1987**, *11*, 663.

(13) Boyle, T. J.; Tyner, R. P.; Alam, T. M.; Scott, B. L.; Ziller, J. W.; Potter, B. G. J. *J. Am. Chem. Soc.* **1999**, *121*, 12104.

Scheme 1

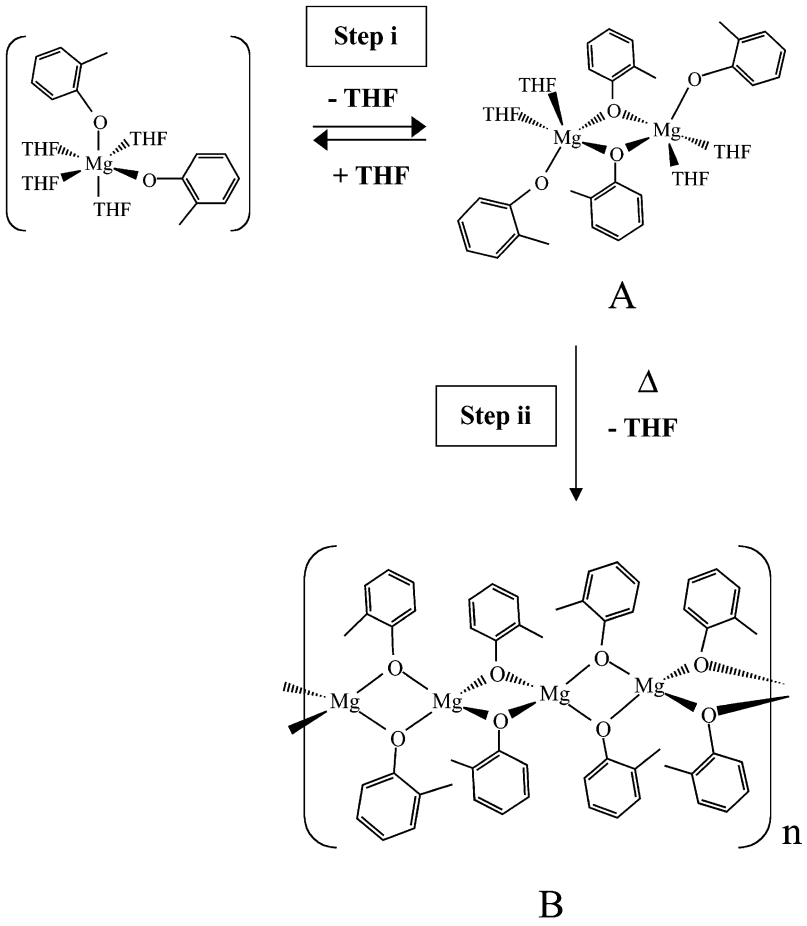

between a monomer and dinuclear species (Scheme 1, step i). This fluxionality may be the source of the solution instability of the dinuclear species that ultimately results in its insoluble, oligomeric destiny.

Morphology Control. As stated previously, we are interested in the preparation of monodispersed, spherical particles for Z−N catalyst supports. Of primary interest is the reduction of PP fines. Since the morphology of the support has been shown to be directly related to the shape of the catalyst and the subsequent PP material,[3] a monodispersed spherical $Mg(OR)_2$ support should reduce the number of PP fines generated. In addition to the shape of the final PP, it is also of interest to control the size of these materials. In the discussion that follows, samples referred to as "better" always possess more spherical particles with less size variation than those to which they are being compared. Throughout this report, we have used the term nucleation to represent the formation of a polymeric $[Mg(oMP)_2]_n$ (**1**) that initiates precipitation and the growth as the subsequent formation of larger particles from these nucleation centers. Several aspects of the reaction can be altered to vary the final particle morphologies.

Since several synthetic pathways had been established for the preparation of **1**, it was necessary to ascertain which route easily and reproducibly generated the desired spherical morphology. Shown in Figure 2 a−c are SEM micrographs of the powders obtained from the reaction mixtures of eqs 1−3. Of these, under the conditions noted in the Experimental Section, the alkyl route (eq 1, Figure 2a) gave the best morphology while the bulk metal route (eq 3, Figure 2c) gave the least desirable product. Therefore, the $Mg(Bu)_2$ route (eq 1) was investigated to determine/optimize its potential for the production of particles. It is of note that under alternative conditions it is expected that spherical particulates could be generated from the other reactions; however, these studies were not pursued.

Early endeavors to reproduce the desirable morphologies produced by the $Mg(Bu)_2$ route proved difficult. When initial attempts were made to reproduce conditions for the original preparation, significant differences in average particle size, particle size distribution, and particle structure were encountered. For example, the microcrystalline morphology that makes up the larger, spherical product particles was significantly altered, as shown in Figure 3. Figure 3a is a micrograph of the surface of the particle from the original sample in Figure 2a. Figure 3b shows a similar micrograph of a duplicate sample (Figure 2a). The sphere in Figure 3a possesses small columnar microcrystallites that appear to grow spherulitically. These changes indicate that crystallite morphologies are subtly dependent on the mechanism of supersaturation and the nucleation and growth that follow (i.e., temperature in this case). To obtain a better understanding of how different experimental parameters affect these processes, the reaction conditions of temperature and concentration were further investigated. In addition, to control precipitation, the use of seeds as nucleation centers was studied.

Concentration Effects. Powders were prepared from solutions at different concentrations of THF. The ulti-

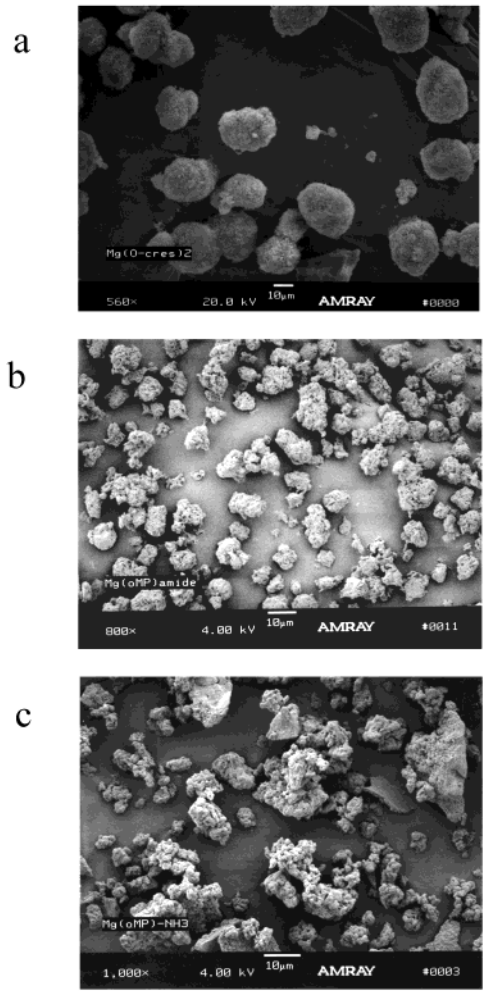

Figure 2. SEM micrographs of powders obtained from the reaction mixtures of (a) alkyl (eq 1, first attempt), (b) amide (eq 2), and (c) ammonia routes (eq 3).

mate morphology of these powders is affected by both the solvent composition and magnesium species concentration. By reducing the concentration of the solution, the particle size distribution (PSD) of the final products broadens in comparison to the original solution concentration. The particles were also found to form at a much higher rate than was originally observed. When the amount of THF was doubled, no precipitate was observed after stirring at room temperature for 12 h. The product was ultimately precipitated by heating the reaction mixture or by vacuum distillation of the volatile portion. The particles produced were less spherical and displayed a broader PSD than the original solution. In general, it was found that changes of ±5% of the baseline concentration would yield spherical particulates whereas any extreme variations proved to be detrimental to the desired spherical morphology.

These results show that solution concentration and solvent will play a dramatic role in influencing the final precipitate's morphology. Changes in concentration will alter the number of nucleation events and affect the kinetics of reaction. By variation of the number of nucleation centers, different growth patterns (growth faces) may be preferred since the rate of consumption of soluble "$Mg(oMP)_2$" (generated by eq 1) would be altered. The particular importance of THF is not surprising since it is incorporated in the intermediate

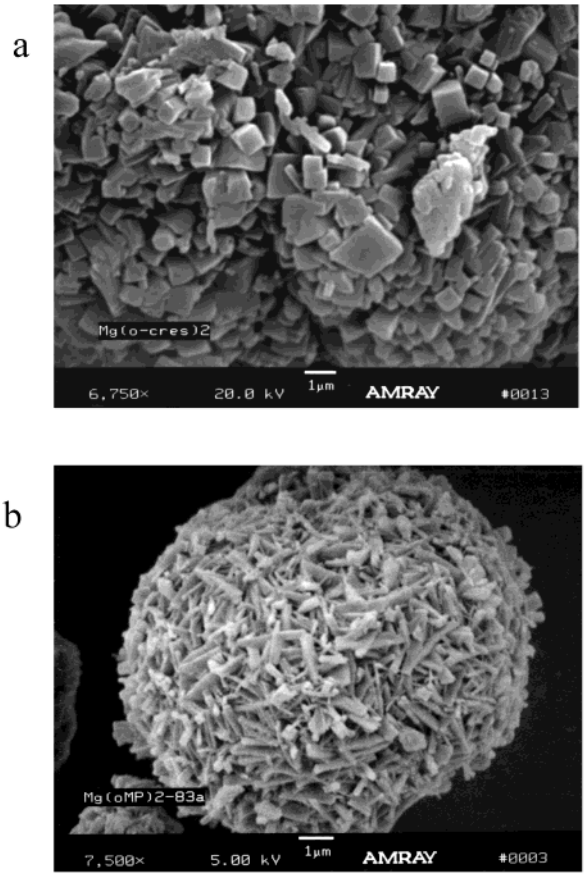

Figure 3. SEM micrographs of high magnification of particles from eq 1 of the (a) first attempt and (b) third attempt.

complex of the proposed precipitation mechanism (Scheme 1). When the amount of THF was halved and the reaction run under the baseline conditions, the faster reaction rate was a consequence of the higher $Mg(Bu)_2$ concentration, which drove the system supersaturation to the point where rapid, uncontrolled nucleation and growth occurred. As a result, precipitates with poor morphologies and broad PSDs were formed. The other extreme is when the reaction was performed under dilute conditions (i.e., doubling the amount of THF). For this case, the precipitation reaction was only initiated either by heating the solution at temperatures well above room temperature (compared to heating the solution from 0 to 12−18 °C for the baseline conditions) or by removal of the volatile portion of the reaction by vacuum distillation (concentrating the solution). It appears that generating a state where precipitation will occur by either of these processes again induces uncontrolled precipitation, leading to products with undesirable morphologies. The solvent concentration "window" for spherulitic growth has been determined to be ≈5% of the THF concentration relative to the baseline reaction.

Temperature Effects. Temperature plays a critical role in controlling the formation of the precipitate by altering the kinetics of the reaction mechanism favoring different nucleation and growth events. For example, a clear baseline solution of **1** was prepared at 0 °C and allowed to precipitate during slow warming to room temperature. A portion of this sample was transferred to a second flask and the solvent removed in vacuo. The remainder of the sample was then heated to reflux

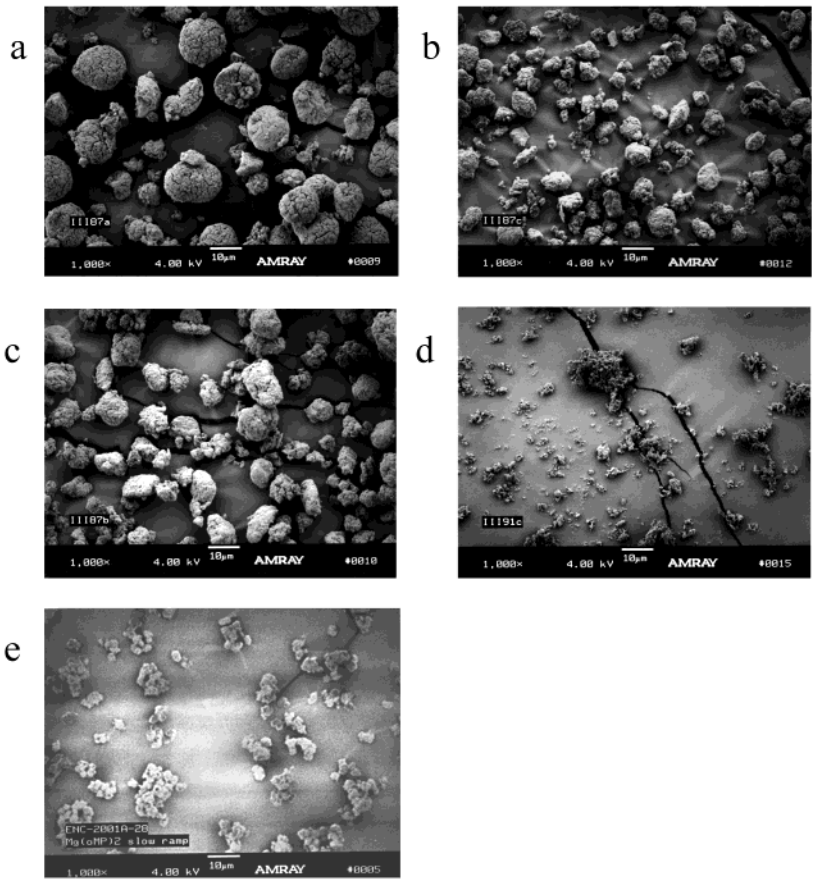

Figure 4. SEM micrographs of **1** powders: (a) ice bath warmed slowly (original method); (b) room temperature (25 °C) water bath; (c) reaction mixture temperature held at 14 °C; (d) hot water (30−53 °C) bath; (e) reaction mixture ramped at 0.1 °C h^{-1} from 12 to 17 °C.

temperature for several hours and isolated by vacuum removal of the solvent. SEM micrographs revealed that elevated temperature conditions are detrimental to the formation of uniform spherical products. This is in comparison to the spherical particles with narrow PSD that were isolated from the original baseline solution, which was allowed to warm slowly from 0 °C to room temperature. Therefore, variations in the rate of the reaction were investigated by altering the temperature of the reaction.

To determine the width of the processing window of an unheated sample of **1**, lower processing temperature regimes were studied. A clear reaction solution was prepared, maintained at 0 °C, and transferred equally into four separate reaction flasks, which were cooled to 0 °C. These flasks were then placed in (i) an ice bath, (ii) a room-temperature water bath (25 °C), (iii) a cold bath initially set at 0 °C, or (iv) a water bath at 30 °C. In a separate experiment (v), a clear reaction solution was prepared and placed in a programmable cooling bath at an initial temperature of 0 °C and was then very slowly warmed to room temperature. All of the solutions were stirred during the course of precipitation. For the ice bath reaction (i), which represents the original method, a precipitate was not observed until the bath temperature reached 18 °C (≈3.5 h), and the resultant powder morphology is shown in Figure 4a. For the reaction placed in a room-temperature water bath (ii), a precipitate was observed after about 20 min and the precipitation was complete after ≈3 h. Figure 4b shows a micrograph of the final powder. The next sample (iii) was placed in a cold bath and left overnight at 8 °C. The temperature of the cold bath was then incrementally raised (1−2 °C/h) and a precipitate was observed only after the bath had reached 13 °C. The reaction was held at 14 °C and precipitation was complete after ≈2 days. The micrograph of the precipitate is shown in Figure 4c. Figure 4d is a micrograph of the sample (iv) that was immediately placed in a heated water bath. The initial temperature of the bath was 30 °C but after 20 min precipitation was believed complete and the temperature had increased to 53 °C. Figure 4e shows the sample (v) obtained after the temperature was raised over a 2-h period from 0 to 12 °C where precipitation was observed to begin. The solution temperature was then ramped to 17 °C at 0.1 °C/h over a 3-day period. The resultant product contained uniform spherical particles of 2−4 μm along with a number of agglomerates.

On the basis of these studies, it was noted that the alteration of the precipitation temperature garnered greater control over the kinetics of precipitation but did not lead to an improvement in particle morphology. It is interesting to note that any sample heated above 15 °C (Figure 4b,d) took about the same time to completely precipitate but the final shape of their product particles are quite different. The final morphologies of these samples indicate that heating has a severe detrimental effect on the final morphology. The sample prepared at low temperature (Figure 4c) took almost 2 days to precipitate but the increased time did not aid the formation of monodisperse spherical particles. All of the

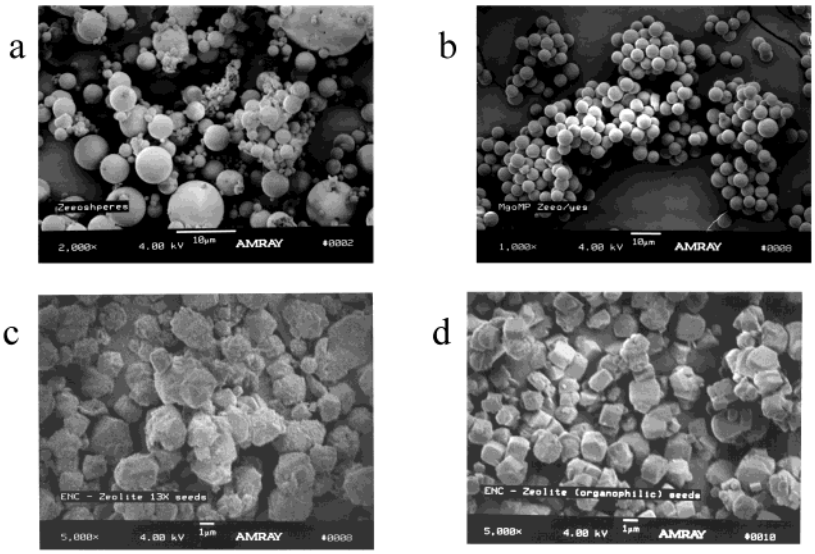

Figure 5. SEM micrographs of seed crystals: (a) Zeeosphere seeds, (b) borosilicate spheres, (c) zeolite Mg-X, and (d) zeolite Mg-MFI.

samples (Figures 4b−e) possess particles with a smaller average diameter than the original conditions (Figure 4a) and are generally less spherical and more random in size and shape. Of the five samples, the best morphology was displayed by the sample that was allowed to warm slowly during precipitation (Figure 4a). Again, this study on the temperature and heating rate effects on morphology illustrate the finite experimental range available for the growth of spherical particles.

Combined, the relatively narrow processing window dictated by the nucleation and growth kinetics is strongly driven by how supersaturation, the initiator of this process, is achieved. For this process, as with other precipitation processes, a relatively high state of supersaturation is required to induce homogeneous nucleation of the product phase. Here, the centers of nucleation can be seen as small polymeric "$Mg(oMP)_2$" complexes that have grown to a sufficient size that further growth while reducing the volume free energy of the system would not offset the increase in surface free energy caused by the formation of the particle surface. For formation of a monodisperse precipitate product, one would ideally form a single burst of particle nucleation (a fixed number of particles) that is followed only by particle growth. Further, to produce spherical particles in a crystalline product, growth should be spherulitic in nature. Qualitatively for this system (Mg-oMP), we have found that slow warming from 0 °C (using appropriate solution concentrations) appears to meet these criteria. Heating too rapidly, for example, increases the supersaturation to such a degree that multiple nucleation events take place and uncontrolled growth occurs.

Seed Crystals. In an attempt to de-couple the need to control both the supersaturation regime of nucleation (high) and growth (moderate) of the spherical particles of **1**, the use of "seeds" as artificial centers of nucleation was investigated. It was thought that the addition of seed particles would reduce the supersaturation levels necessary to induce precipitation since an existing nucleation surface would already be present. Also, the size of the final particle should be dictated by the number of seeds added. The question of what would be an acceptable seed particle was addressed first.

Initial experiments were carried out using five different, commercially available materials as seed crystals: borosilicate glass beads (5.1 ± 0.5 μm from Duke Scientific Corp.), Zeeosphere Ceramic Microspheres (G-200, mean particle size 5 μm from 3M Specialty Materials), zeolite X (type 13X, average particle size 3 μm, from Aldrich), zeolite MFI (average particle size 3 μm, from Aldrich), and polystyrene−divinylbenzene copolymer beads (average particle size 3.2 μm, from Duke Scientific Corp.). These particular materials were chosen due to their spherical, or near-spherical, nature and availability. Figure 5a−d shows the SEM micrographs of the first four types of inorganic seed materials (the polystyrene/DVB copolymer seeds were found to result in no significant improvement of particle size or morphology and will not be discussed further). The polydisperse Zeeosphere seeds, which have an alumina−silica composition, are shown in Figure 5a, with diameters ranging from 0.5 to 15 μm. The essentially monodisperse 5.1-μm-diameter borosilicate glass spheres are shown in Figure 5b. The two aluminosilicate zeolite materials possess a narrow polydispersity and exhibit different hydrophobicities: zeolite-X (Figure 5c) is relatively hydrophilic due to the high aluminum content of its framework, while the more siliceous zeolite-MFI (Figure 5d) is hydrophobic. Prior to use as seeds, the zeolite powders were repeatedly treated with aqueous magnesium chloride solution (0.05 M) at room temperature followed by a wash with deionized H_2O to exchange the charge-balancing cations (predominantly Na^+) in the zeolite structure with Mg^{2+}. This was done to avoid any influence of foreign cations on the nucleation and growth of the particles of **1**. As well as using foreign seed materials, the addition of freshly prepared **1** particles to a precursor solution prior to particle formation (self-seeding) was also investigated.

To control the size and number of particles through the use of seed crystals, it is necessary to rely on one important assumption: there is a one-to-one correlation between the number of seed crystals and number of

product particles. That is, every product particle must have one seed crystal embedded in it. This is not unreasonable, as it is generally accepted, that the growth of a particle on an existing surface requires less energy than a new nucleation event. Therefore, under the proper conditions, heterogeneous (growth on seeds) nucleation may be favored over homogeneous (growth from new nucleation centers) nucleation. With this assumption, only a few physical properties must be known to calculate the mass of the seeds (m_s) required to yield product particles of a chosen average radius (r_p, see eq 5). The necessary data, in addition to the expected total mass of the product (m_p), includes the densities of both **1** (d_p) and the seeds (d_s) and the average radius (r_s) of the seeds.

$$m_s = m_p\left(\frac{V_s}{V_p - V_s}\right)\left(\frac{d_s}{d_p}\right) \tag{4}$$

$$m_s = m_p\left(\frac{r_s^3}{r_p^3 - r_s^3}\right)\left(\frac{d_s}{d_p}\right) \tag{5}$$

The volume of the product contained in a single particle is obtained by subtracting the volume of the seed from the total volume of the final particle in which it is embedded. Since it is the ratio of volumes that is important, the equation simplifies to the multiplicative outcome of the mass of the product, the relative cubed radii of the seeds and the difference between the cubed radii of the total particle and seed, and the relative densities of the seeds and product (eq 5).

To control the precipitation, or nucleation event, it is important that the seeds be added to the solution before the onset of precipitation. Therefore, with use of eq 5, an appropriate amount of Zeeosphere seeds, glass beads, or zeolites were added to several flasks that were then placed in an ice bath. A clear, cooled (≈0 °C), colorless solution of **1** was equally distributed to the seed-containing flasks and the precipitation initiated under the conditions described below. An additional implication from eqs 4 and 5 is that for a given mass of product the volume of **1** surrounding each seed must decrease as the seed concentration increases. The products from the experiments using (i) Zeeosphere seeds and glass beads, (ii) zeolites-X and -MFI, and (iii) self-seeding are discussed below.

(i) Zeeosphere Seeds and Glass Beads. SEM micrographs of a Zeeosphere seed and a glass bead embedded in **1** are shown in parts a and b, respectively, of Figure 6. These pictures illustrate the proof of principle that the product will nucleate and grow around a seed particle. Keeping the expected product mass constant, 5.1-μm-diameter glass spheres were added to two flasks to give final average diameter particles of 20 and 12 μm. While both samples possess smaller average diameters than expected, the sample containing fewer seed crystals did yield larger particles. The samples of **1** prepared in the presence of Zeeosphere seeds and glass spheres were found to be similar. Therefore, the use of more polydisperse seeds did not correlate to visibly more polydisperse product particles.

Attempts to generate 20-μm particles yielded particle sizes that were significantly less than expected. These consistently smaller than predicted particles suggest

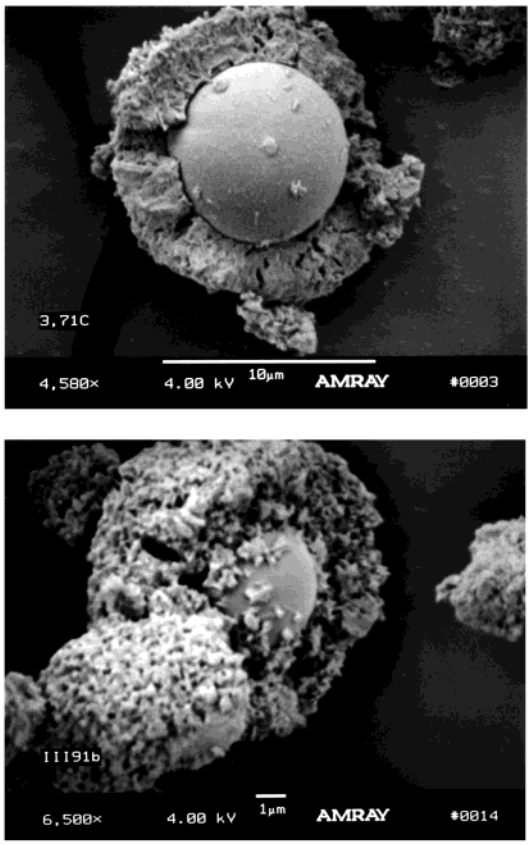

Figure 6. SEM micrographs of seeded growth of **1** around (a) Zeeosphere seeds and (b) borosilicate glass.

that the initial assumption of a one to one correlation between seed and particle is not correct. A particularly insidious dilemma may be the concurrence of **1** nucleating both hetero- and homogeneously. If this is the case, then the only alternative is to suppress heterogeneous nucleation. Seed surface modification is one approach that may accomplish this suppression. If the surface could be altered to be "stickier" or to promote heterogeneous nucleation, then homogeneous nucleation may become statistically less favored. Additionally, careful temperature control may correlate to increased kinetic control of precipitation and thereby also improve the probability of heterogeneous nucleation. Alternatively, nucleation and growth may initially begin on the seed surface but **1** may peel away before the coating becomes thick enough to be self-reinforced. Slower stirring speeds or "stickier" seeds may be two possible means by which to suppress these problems.

In an effort to modify the seed surface or the reaction kinetics governing nucleation and growth, the Zeeosphere seeds were treated with different reagents prior to addition of the solution of **1**. The potential modifiers are standard components in many Z−N PP catalytic systems.[1−3] The general procedure included adding 50% (w/w) of the reagent material to the seeds and 1 mL of toluene to ensure that the reagent dissolved. Electron micrographs of the precipitated **1** onto seeds modified with toluene and ethyl benzoate (EB) are shown in parts a and b, respectively, of Figure 7. The use of EB had a significant influence on the microstructure of the particle surface; instead of the needlelike microcrystallites seen in Figure 7a, the microcrystallites in Figure 7b

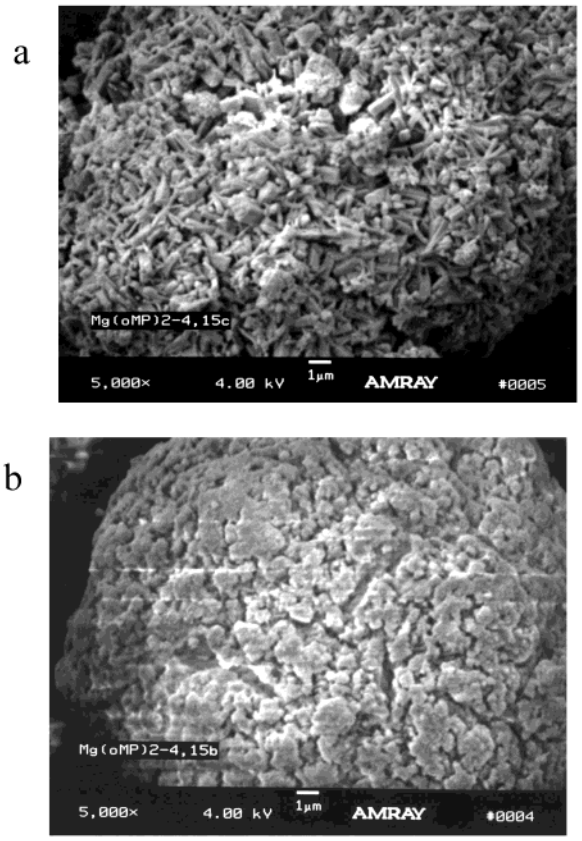

Figure 7. SEM micrographs of Zeeosphere seeds (20-μm level) pretreated with (a) toluene and (b) ethyl benzoate.

have the appearance of having been flattened and melted together. Pretreatment with toluene only had a positive effect on the final morphology; the particles appear generally larger, on average, than seen in previous experiments.

A second set of experiments was undertaken using the following modifiers: (a) toluene (repeat), (b) chlorobenzene (CB), and (c) di-*iso*-butyl phthalate (DBP), (50% w/w) and 1 mL of toluene. All three experiments gave spherical, relatively monodisperse **1** particles. Lower magnification electron micrographs, which emphasize this outcome, can be viewed in Figure 8a (toluene), 8b (CB), and 8c (DBP). It appears that changing the electronics of the aromatic ring (toluene v. CB) did not alter the positive effect of the added aromatic. One explanation of this significant improvement through the introduction of aromatic species is the concept of microprecipitation at the surface of the particle (note: **2** is not soluble in toluene and will preferentially precipitate in its presence).

A series of experiments was performed with different concentrations of Zeeosphere seeds, pretreated with toluene, to optimize the system in terms of particle size and particle size distribution, as illustrated in Figure 9a−e. The sample prepared without seed addition (Figure 9a) possesses near-spherical particles 5−10 μm as well as some smaller particulates. Addition of 1 equiv of seeds (an equivalent is defined here as the quantity of seeds, calculated using eq 5, required to yield a product containing 20-μm-diameter particles) produced a sample containing near-spherical particles of 10−20−μm diameter (Figure 9b). Increasing the seed concentration to 1.5 equiv (eq 5 predicts 17.5-μm particles)

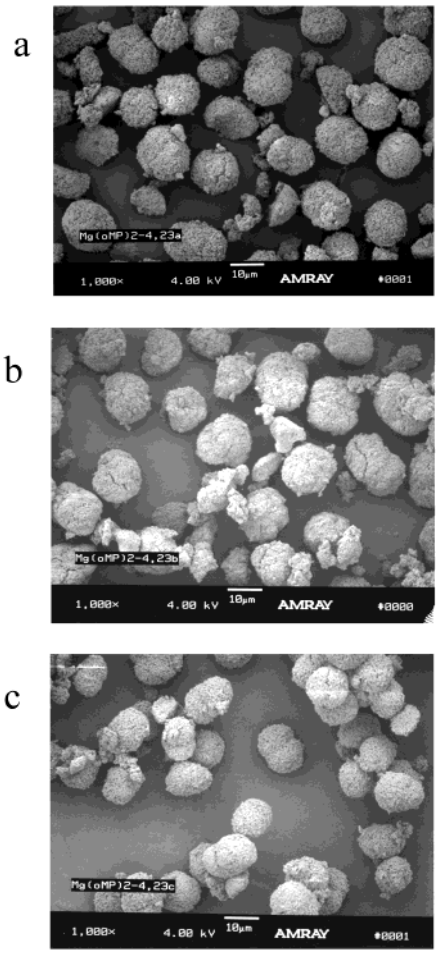

Figure 8. SEM micrographs of **1** around Zeeosphere seed (20-μm level) pretreated with (a) toluene, (b) chlorobenzene, and (c) dibutyl phthalate.

produced a significant decrease in particle size to 8−15 μm (Figure 9c), while further increases in seed concentration to 2 and 3 equiv (eq 5 predicts 16 and 14 μm, respectively) brought about minor decreases in particle size (see parts d and e, respectively, of Figure 9). All of the samples in Figure 9 contain irregular particles <5 μm in size. However, the relative amount of these fine particulates was found to decrease as the seed concentration increased; at seed concentrations above 1.5 equiv, fine particulate formation was minimal. This observation indicates that there is competition between hetero- and homogeneous nucleation of particles of **1**. Once the available seed surface area reaches a sufficiently high value, homogeneous nucleation is essentially suppressed. This phenomenon can be rationalized if the assumption is made that the seed surface offers a more favorable growth surface than already-formed **1**. When a low concentration of seeds is present, the available seeds are soon coated by **1**, at which point the driving force for seed growth is reduced; however, when a higher seed concentration is present, the concentration of **1** precursor in solution (or degree of supersaturation) becomes depleted to a much greater extent before the seeds are coated, thus reducing the tendency for homogeneous nucleation. Thus, a tradeoff exists between the generation of large particles (1 equiv of seeds) and the minimization of fines (>1.5 equiv). Another consequence of high seed concentrations is the

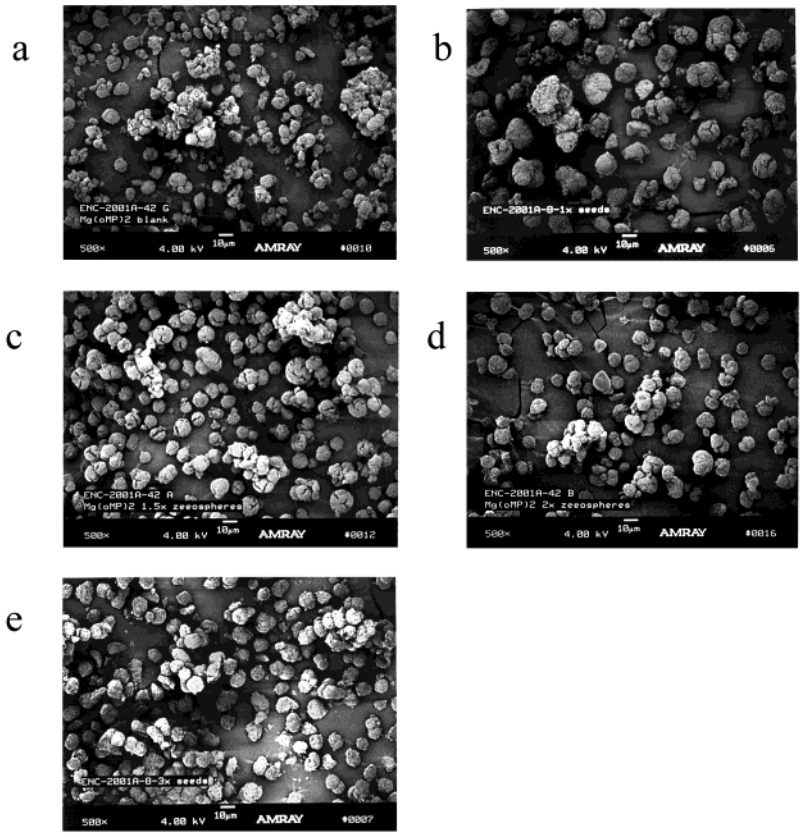

Figure 9. SEM micrographs of **1** grown in the presence of various concentrations of Zeeosphere seeds: (a) No seeds; (b) 1 equiv (predicted size from eq 5: 20 μm); (c) 1.5 equiv (predicted size: 17.5 μm); (d) 2 equiv (predicted size: 16 μm); (e) 3 equiv (predicted size: 14 μm).

observance of uncoated seeds in the final precipitated material. This is due to the relatively thin coating of **1** that is less rigid and can therefore delaminate more easily during handling than the thicker coatings obtained at lower seed additions.

(ii) Zeolites-X and -MFI. Since surface modifications appeared to have a significant effect on the final morphology, seed crystals with inherently different surface characteristics were investigated. Since many zeolites naturally absorb ambient moisture, zeolites-X and -MFI were dried under vacuum at ≈200 °C and stored under an inert atmosphere prior to use. Attempts to utilize the hydrophilic zeolite-X seeds without this dehydration step yielded a poor product, while the hydrophobic zeolite-MFI seeds produced an acceptable product. Parts a and b of Figure 10 show the products obtained using zeolite-X and -MFI, respectively, at a concentration calculated (eq 5) to yield 19-μm-diameter particles. The samples are polydispersed spherical particles in the range 8−20 μm, similar to that seen in the Zeeosphere-seeded system under identical concentration (Figure 9b). In contrast to the previous seeds investigated, it is not possible to visually detect the delineation between the zeolite seed and the **1** particle; however, energy-dispersive spectroscopy (EDS) analysis of zeolite-seeded samples was unable to detect Si or Al from the zeolite, confirming that the seeds are all coated with **1**. Furthermore, toluene appeared to have a negligible affect on product morphology and uniformity when using the zeolite seed. Thus, it is apparent that surface-modified zeolites may also be suitable seeds for the growth of Z−N catalyst precursors.

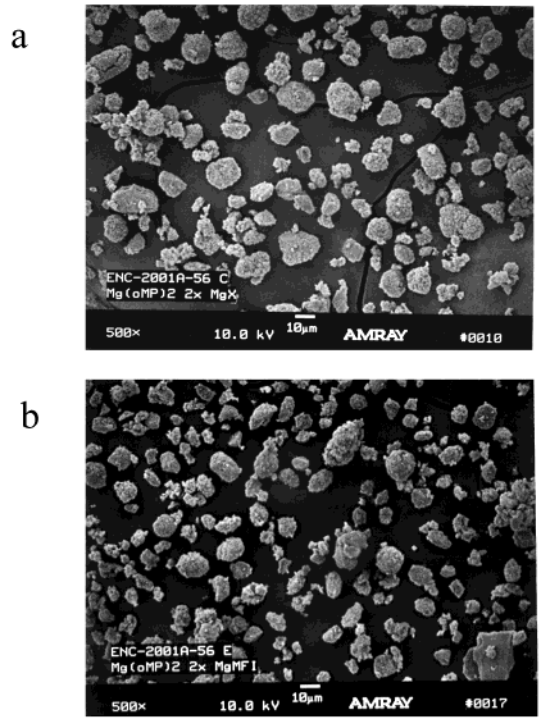

Figure 10. SEM micrographs of **1** grown in the presence of zeolite seeds, at a concentration calculated to yield 19-μm-diameter particles. (a) Zeolite Mg-X seeds and (b) zeolite Mg-MFI seeds.

(iii) Self-seeding. In an effort to avoid dilution of the final Z−N catalyst by (catalytically inert) seed material and due to the lack of a seed:**1** interface observed for

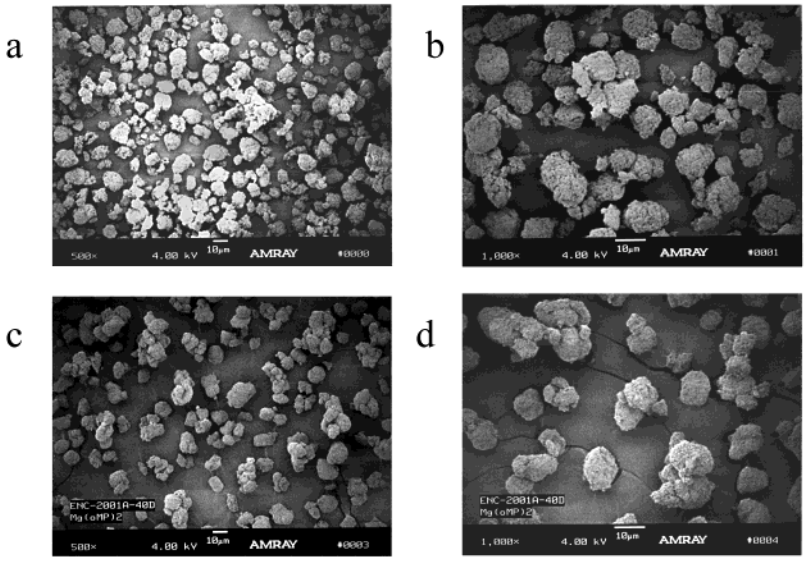

Figure 11. SEM micrographs of self-seeded **1** and parent material. (a) and (b) particles obtained from the precipitate which was used to seed the growth of (c) and (d).

the zeolites, it was of interest to attempt seeding with preformed **1**. An experiment was undertaken in which freshly prepared **1** particles (still in their mother liquor) were introduced into a fresh **1** solution prior to precipitation. This self-seeded mixture was allowed to precipitate as normal and was then re-cooled to 0 °C. One-quarter of this material was transferred via cannula to a second, fresh solution at 0 °C and the remainder of the precipitated material was dried as normal. Addition of the preformed **1** particles to the fresh solution did not induce spontaneous precipitation of **1** nor was there any significant dissolution of the particles. The particles/fresh reaction mixture was then allowed to warm to room temperature and precipitate out as before. SEM micrographs of the resulting particles are shown in Figure 11a−d. The material prepared without seeding (Figure 11a,b) possessed 10−15-μm spherical particles as well as some fine particulates (typical for an unseeded sample or for a sample prepared with only small quantities of seeds). While there is not a significant increase in the size of the spherical particles in the self-seeded material (Figure 11c,d), the bulk powder does show better uniformity (i.e., less fine particulates and a narrower PSD) than the unseeded material. The reduction in concentration of fine particulates indicated that growth onto the existing **1** particles is more favorable than homogeneous nucleation under these conditions.

Conclusions

We have prepared "$Mg(oMP)_2$" that can be isolated as a polymeric solvent-free species, **1**, or as a dinuclear THF adduct, **2**. While thermodynamics favors the polymeric form, the dinuclear complex can be stabilized when dissolved in neat THF. Additionally, the polymeric species can be redissolved in the presence of a sufficiently strong Lewis base (e.g., pyridine). Synthesis of $[Mg(oMP)_2]_n$ (**1**) from $Mg(Bu)_2$ in an ice bath that was allowed to slowly warm to room temperature led to the formation of a precipitate comprised mainly of spherical particles. While many variables can influence the spherical nature and PSD of these particles, it was determined that highly concentrated or diluted reaction mixtures adversely affect the desired properties of these particulates. Furthermore, maintaining high or low temperatures yielded poorly shaped particles while a slow transition through the precipitation point yielded highly spherical particulates. Addition of seed crystals to a solution of **1** resulted in the nucleation and growth of the precipitate around the seed. Three seeding systems have demonstrated control over particle morphology and size: (1) the use of toluene in the presence of the Zeeosphere seeds; (2) the use of zeolite seeds; and (3) self-seeding with freshly prepared particles of **1**. The first seeds showed a distinct delineation between the seed and the particle growth that was not observed for the other two seeds. These approaches show promise for morphology control during precipitation and may allow for the tailoring of particle size in a number of other systems.

Acknowledgment. For support of this research, the authors would like to thank the Office of Basic Energy Science of the Department of Energy and the United States Department of Energy under Contract DE-AC04-94AL85000. Sandia is a multiprogram laboratory operated by Sandia Corporation, a Lockheed Martin Company, for the United States Department of Energy.

Supporting Information Available: Experimental data for **2** (PDF). A listing of the X-ray crystallographic information for **2** (CIF). This material is available free of charge via the Internet at http://pubs.acs.org.

CM020802O